13th IEA Heat Pump Conference
April 26-29, 2021 Jeju, Korea

Study on the frosting phenomena between concavity and convexity plate under forced convection - The prediction of frost layer growth using the observation from the frost and defrost multi-cycle experiment-

Masafumi Katsuta[a],Shota Ikutaya[b], Yuki Terakado[b], Junya Yamagishi[b], Rio Asakawa[b] , Sangchul Bae[a]

[a]*Department of Modern Mechanical Engineering, Waseda University, Shinjuku-ku, Tokyo, 169-8555, Japan*
[b]*Graduate School of Environment and Energy Engineering, Waseda University, Shinjuku-ku, Tokyo, 169-8555, Japan*

Abstract

Recently, the development of hybrid and electric vehicles has been promoted. Along with this, since the impact reduction for cruising distance and the securing of the heat source are problems, changes are also required for the air conditioner. Therefore, high efficiency of the air conditioning system by improving efficiency of the heat exchanger has become more necessary. However, due to frost formation of the outside heat exchanger in a cold climate region, increase of pressure drop and decrease of heat transfer rate are supposed to be an application difficulty of HP systems.

The objective of this study is to analyze the mechanism of frosting phenomenon in a fin-less heat exchanger. This is intended to clarify the advantage in terms of frost strength and defrosting performance of a fin-less heat exchanger.

In this research, the frost and defrost multi cycle experiment are established and the qualitative characteristics are investigated. Through observation of frost layer growth in the continuous experiment, ice column growth such as initial ice column diameter and ice column distance is grasped and influence of wettability on ice column growth is also confirmed.

Keywords : Frosting and Defrost Phenomena under Convection, The effect of Wettability Frost Layer Growth, Finless Heat Exchanger;

1. Introduction

Currently, as a power train alternative to gasoline and diesel vehicles in the automotive industry, the development of hybrid and electric vehicles has been promoted. Along with this, since the impact reduction for cruising distance and the securing of the heat source are problems, changes are also required for the air conditioner. Therefore, high efficiency of the air conditioning system by improving efficiency of the heat exchanger and changing to hat pump system has become more and more necessary. However, due to frost formation of the outside heat exchanger by using in the cold climate region, increase of pressure drop and decrease of heat transfer rate are expected to be a problem on HP systems.

Multi-flow type heat exchanger having a corrugated-louvered fin is the mainstream of the heat exchanger for a vehicle, and the fin and tube miniaturization is progressing in order to improve the performance. Thereby, since the retention amount of the condensed water or melting water between the fins increases, frost strength and defrosting performance is feared to be reduced. As improved method for these problems, fin-less type heat exchanger has been proposed to prevent the retention of condensate. This study is to analyse the mechanism of frosting phenomenon in fin-less heat exchanger, it is intended to clarify the advantage in terms of frost strength and defrosting performance fin-less heat exchanger for the current heat exchanger.[1)-3)]

2, Methodology

2.1. Experimental Apparatus

Fig.1 is a schematic diagram of experimental apparatus. Experimental apparatus is composed of constant temperature and humidity air chamber, blower, orifice flow meter, test section and the duct. The air controlled by temperature and humidity from the chamber, is flowing into the test section by the blower and then returned to the chamber. Air temperature and humidity before and after the test section is measured by the temperature and humidity sensors. In addition to the area of frost layer, diameter and interval distance of crystal columns were measured by using an image processing. Experimental system is almost same as previous paper.(paper number) To establish the defrosting condition, the hot water heating is adopted and its system is shown in Fig.2.

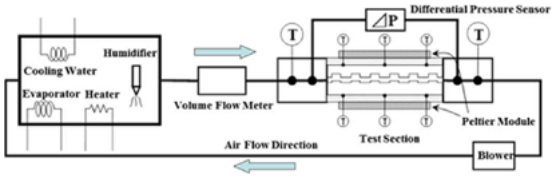

Fig. 1. Schematic of Experimental Apparatus

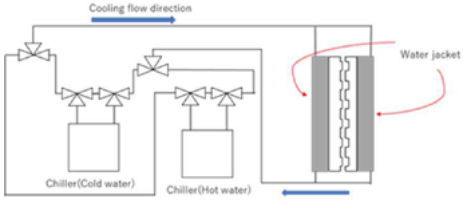

Fig. 2. Circuit diagram including Water Jacket (Defrost)

2.2. Test Section

Fin-less heat exchanger has a shape like Fig.3. In this study, we focus on the air side passage, and a test section focusing on only one flow path is prepared as shown in Fig.4. Test section has a periodic convex-concave shape as shown in Fig.5, and the size of each part is defined as shown in Fig.6.

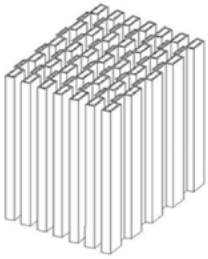

Fig.3. General View of Heat Exchanger

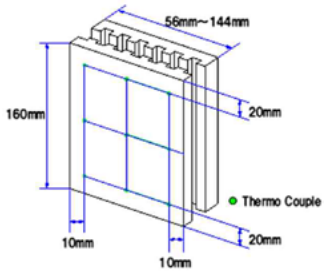

Fig.4. Test Section Plate

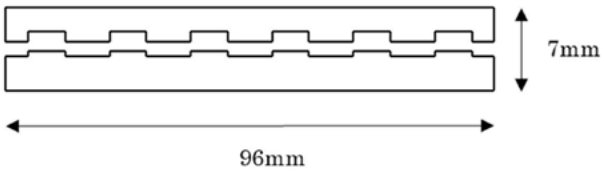

Fig.5. Flow Channel of Test Section

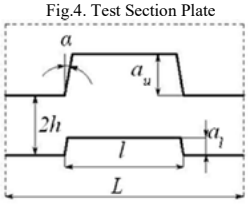

Fig.6. Detail of Flow Channel

2.3 Experimental methodology and condition

First, air conditions in the air chamber are adjusted to the experimental aimed value as shown in table 1. Turn off the blower after confirmation of the steady state, and the test section was cooled down to a set temperature. The experiment started after reaching the set temperature, and to measure the temperature, humidity and pressure drop across the test section until channel blockage, and the state of frost growth was taken by camera. Then, the test section was removed, and frost weight was measured. Air flow rate decreases in accordance with frost growth, however the blower output was fixed. Design parameters of test section are shown in Table 2.

After the end of each experiment, the height of the frost layer was taken by camera from the top of test section, and the height of the frost layer was measured. The captured image can be incorporated into image processing and analysis software, and then the height of frost layer is measured.

Table 1. Experimental Conditions

Temperature	℃	7.0
Temperature of Cooling Surface	℃	−10.0
Relative Humidity	%	86.0
Initial Air Flow Rate	m^3/h	5.0

Table 2. Design Parameters of Test Section

			No.1	No.2	No.3	Hydrophilic	Hydrophobic
Height of Convexity Portion	a_l	mm	2.0	1.2	2 .8	2.0	2.0
Depth of Concavity Portion	a_u	mm				2.8	
Length of convex-concave portion	l	mm				8.0	
Pitch of convex-concave	L	mm				16.0	
Taper Angle of Unevenness	α	deg				10	
Number of convex-concave	N	—				6	
Contact Angle (Wettability)	-	deg		60~90		~10	150~

3. Result and Discussion

3.1. The heat transfer rate and pressure drop

The channel blockage time is the time until the air flow rate becomes zero or the increase rate of the approximate curve of the air flow rate becomes zero.

The purpose of the experiment was to clarify the effects of the height of the convex part and the surface treatment, focusing on the pressure loss and the amount of heat absorption, in the air flowing through the test section simulating a row of concave and convex plate. Obtained experimental result is substituted for the following equation and the heat transfer rate is calculated.

$$\dot{Q} = \dot{Q}_s + \dot{Q}_l = \dot{m}_a C_p \Delta T + \dot{m}_a \Delta W (\hbar_{fg} + \hbar_{fg}') \quad (1)$$

h_{fg}: Latent heat of condensation h_{fg}': Latent heat of solidification

However, since the amount of water whose state changed from water to ice is unknown from the experimental results, Equation (1) is calculated on the assumption that all the water amounts obtained from the absolute humidity difference are frozen instantly.

3.2. The heat transfer rate of each flat plate

This experiment consists of 2 cycle frost and defrost experiment. The result of the convex-concave flat plate with different heights and the wettability is shown from Fig.7. to Fig.11. Fig.12. and Fig.13. show total heat flow rate.

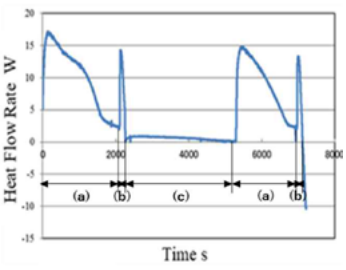

Fig. 7 Heat Flow Rate of No.1 Plate

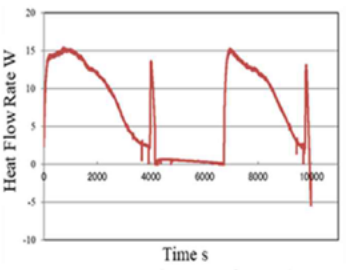

Fig. 8 Heat Flow Rate of No.2 Plate

(a)Frosting Period
(b)Defrosting Period
(c)Preparing Period

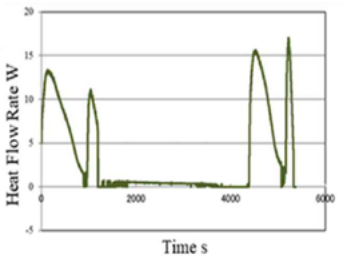

Fig. 9 Heat Flow Rate of No.3 Plate

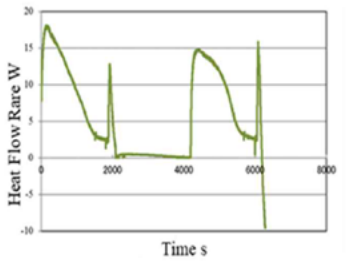

Fig. 10 Heat Flow Rate of Hydrophilic Surface

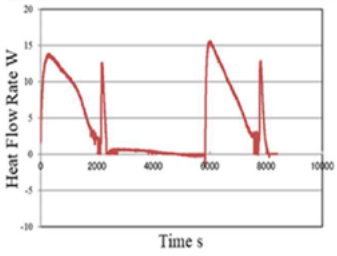

Fig. 11 Heat Flow Rate of Hydrophobic Surface

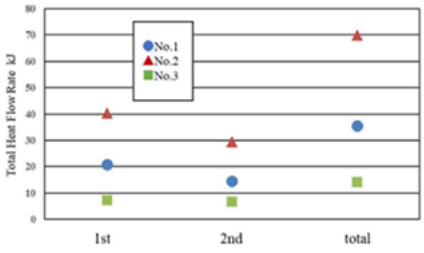

Fig. 12 Total Heat Flow Rate (Comparison with Convex Height)

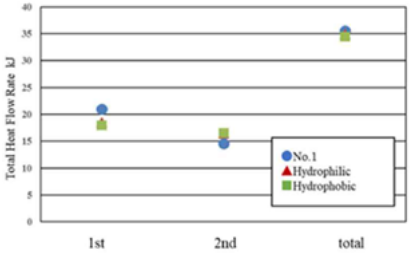

Fig. 13 Total Heat Flow Rate (Comparison with Surface Condition)

From Fig. 12, No.2 experimental convex-concave plate having the lowest height achieves the highest heat flow rate. Also, from Fig.13, the surface treatment (difference wettability) does not have the clear effect on heat flow rate.

3.3. Blockage arise time of each experimental convex-concave plate

The channel blockage time is the time until the air flow rate becomes zero or the increase rate of the approximate curve of the air flow rate becomes zero. Fig.14. to Fig.22. show that the pressure drop of second cycle compared with height and wettability as the parameter.

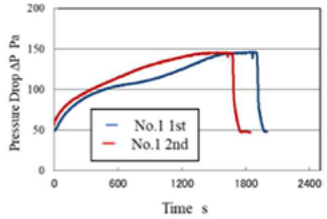

Fig. 14 Pressure Drop of No.1 Plate

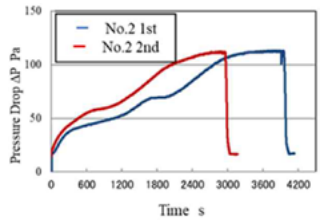

Fig. 15 Pressure Drop of No.2 Plate

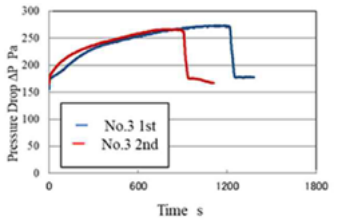

Fig. 16 Pressure Drop of No.3 Plate

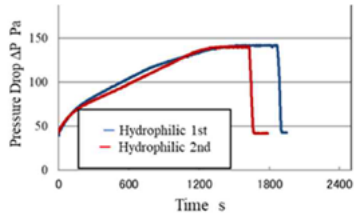

Fig. 17 Pressure Drop of Hydrophilic Surface

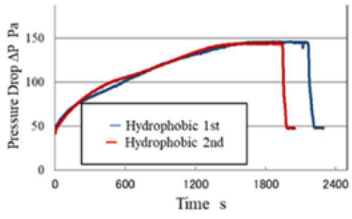

Fig. 18 Pressure Drop of Hydrophobic Surface

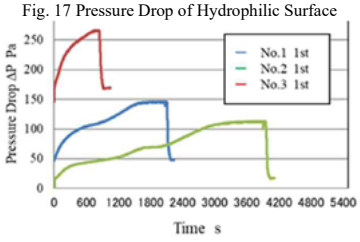

Fig. 19 Pressure Drop of 1st Cycle

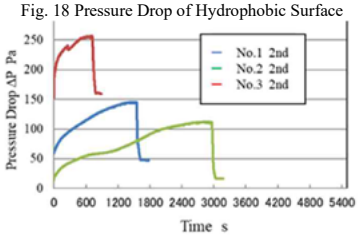

Fig. 20 Pressure Drop of 2nd Cycle

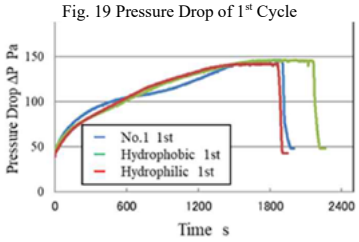

Fig. 21 Pressure Drop of 1st Cycle

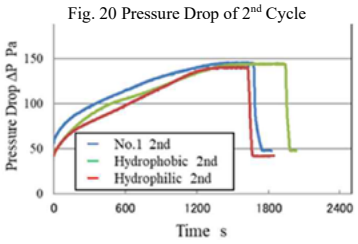

Fig. 22 Pressure Drop of 2nd Cycle

Each test piece plates, second cycle experiment is earlier to close as shown from Fig.14. to Fig.20. Comparison is made by wettability; the hydrophilic plate is earlier to close than other test pieces (Fig.21 and Fig.22).

3.4. Observation of Frost Crystals Growth

By changing the one side of the aluminium plate to acrylic plate, the test section was visualized. After frost crystals appear, the interval distance and diameter distance were measured. Fig.23. is shown No.1 plate, Fig.24. is shown hydrophobic plate and Fig, 25. is shown hydrophilic plate.

(a) Initial condition (No.1)

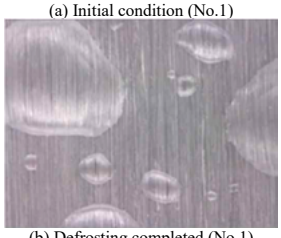

(b) Defrosting completed (No.1)

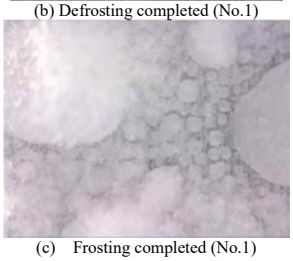

(c) Frosting completed (No.1)

Fig. 23. Observation of Frost Crystals Growth (No.1)

(a) Initial condition

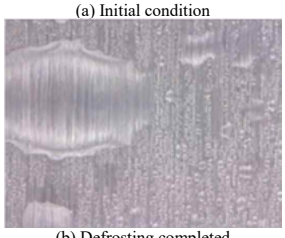

(b) Defrosting completed

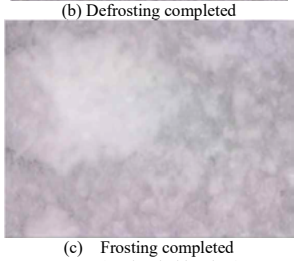

(c) Frosting completed (Hydrophobic Plate)

Fig.24. Observation of Frost Crystals Growth (Hydrophobic)

(a) Initial condition

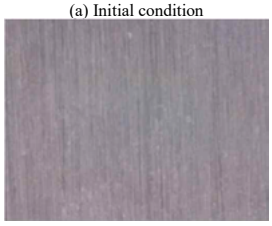

(b) Defrosting completed

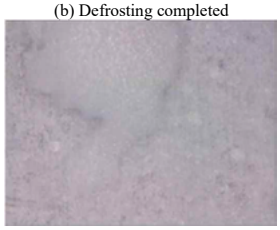

(c) Frosting completed (Hydrophilic plate)

Fig.25 Observation of Frost Crystals Growth (Hydrophilic)

The air flows from right to left on test piece. The hydrophilic test section has different trend to compare with other test pieces. In the first cycle, it is confirmed that droplets are generated like the other test pieces and ice crystals grow from there. However, in the second cycle, it is confirmed that the frost crystals are growing as they were without small droplets coalescence each other. Moreover, after the defrosting is completed, the generation of droplets is observed in other test pieces, but this hydrophilic test piece is not so clear as compared with the other test pieces. Much more in detailed observation movies will present in conference.

Next, the initial crystal column diameter and ice column interval are measured using image processing in the same manner as the frost layer area measurement for the frost column in each channel taken by frost layer growth observation. The initial crystal column diameter is measured when the formation of frost columns is confirmed growing with ice droplets as the nucleus. The number of ice droplets is counted for the crystal interval, and the interval is defined as the distance between crystals assuming that it is uniformly distributed in an image area. However, since it is difficult to count the number of ice droplets in the second cycle of hydrophilic test piece, the distance between the ice drops that could be confirmed is taken as the ice column interval. The future task is to improve the accuracy of the measurement method of ice column diameter and ice column interval. The measured ice column diameter and ice column interval are summarized in Table 3.

Table 3. Various amounts of initial frost crystals forming

	1st Initial crystal column diameter (mm)	1st Crystal column interval (mm)	2nd Initial crystal column diameter (mm)	2nd Crystal column interval (mm)
No.1	0.015	0.051	0.022	0.063
Hydrophobic	0.025	0.065	0.021	0.060
Hydrophilic	0.013	0.054	0.007	0.036

3.5 Analysis of frost layer growth

The growth process of the frost layer is classified into “Crystal growth stage”, “Frost layer growth period”, and “Frost layer full growth stage”. Crystal growth stage: Needle-like crystals are generated with ice droplets as nuclei, forming crystals, forming a frost layer with a large porosity and rough surface. Frost layer growth stage: Side branches occur on the side of the frost column, filling the voids, forming a frost layer with a small surface roughness and a flat surface The calculation is based on Yamashita's model[7], which is obtained by multiplying a constant to Tao et al [6]. Water vapor transport through the frost layer considered to be a porous layer and is divided into a frost layer density increasing component and a frost layer height increasing component that diffuse inside the frost layer according to the concentration gradient. As mentioned, using analysis method is almost same as previous paper[4]. Here important key equations[5)-8)] are summarized as below .

$$(\delta L_f/\delta t) = C_2 \times (h_D / \rho_I) \times (X_a - X_{fs}) \quad (2)$$

$$(\delta d/\delta t) = C_3 \times 2 \times (h_D / \rho_I) \times (X_{\ddot{y}} - X_I) \quad (3)$$

$$T_Y = k_\alpha \times T_\alpha + (1 - k_\alpha) \times T_w \quad (4)$$

$$\rho_f = \frac{\int_0^{Lf} [\frac{\pi}{4} d^2 \rho_I + (l^2 - \frac{\pi}{4} d^2) \times \rho_a] \times dz}{l^2 \times Lf} \quad (5)$$

h_D = Mass transfer coefficient [kg / m^{2}sΔX] , X_{fs} = Absolute humidity of Frost Layer Surface [kg / kg´] X_f = Absolute humidity of frost layer [kg / kg´], k_a ・ C_2 ・ C_3: Constant , X_a = Absolute humidity of air [kg /kg´] d = Crystal column [m] , X_l = Absolute humidity crystal column [kg / kg´]

$$\dot{m} = \dot{m}_d + \dot{m}_h = h_D \times (X_a - X_{fs}) \quad (6)$$

$$\varepsilon = \frac{\rho_i - \rho_f}{\rho_i - \rho_a} \quad (7)$$

$$\dot{m}_d = D_{eff} \times \frac{d\rho_v}{dz} = D_{eff} \times \frac{M_v}{RT_f} \times \frac{dP_v}{dz} \quad (8)$$

$$D_{eff} = \mu \times D_v = \frac{\varepsilon}{\tau} \times D_v \quad (9)$$

$$\partial \rho_f / \partial t \times (t_f \times A_w) = \dot{m}_d \times A_w \quad (10)$$

Table 4. The Suggested Formulas of Tortuosity

Year	Name	Tortuosity
1969	Brian et al	$\tau=1.1$
1986	Auracheret al	$\tau=1-0.58\times(1-\varepsilon)$
1993	Taoet al	$\tau=1/1.1$
1997	Le Gall et al [9)]	$\tau = \frac{\varepsilon}{\frac{\varepsilon}{1-0.58\times(1-\varepsilon)} + F\times 10\times(1-\varepsilon)\times\varepsilon^{10}}$
2002	Mezedure et al	$\tau = \frac{\varepsilon}{1-(1-\varepsilon)^{0.5}}$

$\dot{m}$: Mss flux kg/m^{2}s $\dot{m}_d$:Mass flux by using density increment kg/m^{2}s $\dot{m}_h$:Mass flux by using increment of the frost height kg/m^{2}s D_{eff}: Effective diffusion coefficient m^2/s Aw : Cooling surface area m^2 μ: Diffusion resistance coefficient ε: Porosity Dv: Diffusion coefficient m^2/s τ:Trtuosity

3.5 Results of analysis

Ice column interval and initial ice column diameter is set as initial value referred to experimental result in Table 3. Table 5 shows the value used in calculation, Fig.26 and Fig. 27 shows the calculation results of the frost density, and Fig. 28 and Fig. 29 show the calculation results of the frost height, respectively.

Table 5. Calculation Parameter

	Transition Region		Crystal Growth Stage				Frost Layer Growth Period
	Starting Time	Closing Time	1st Initial ice column diameter mm	1st Ice column interval mm	2nd Initial ice column diameter mm	2nd Ice column interval mm	Tortuosity
No.1	60s	1170s	0.015	0.051	0.022	0.063	Le Gall et al eq.(F=1)
Hydrophobic			0.025	0.065	0.021	0.060	Le Gall et al eq.(F=1)
Hydrophilic			0.013	0.054	0.007	0.036	Le Gall et al eq.(F=1)

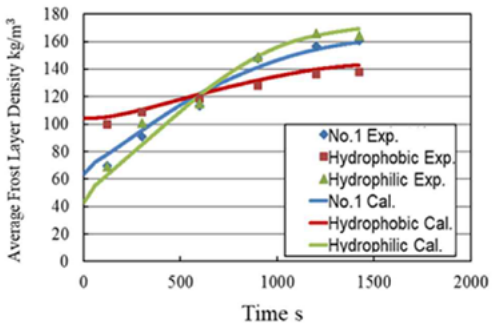

Fig.26. Average Frost Layer Density as Function of Time (1st)

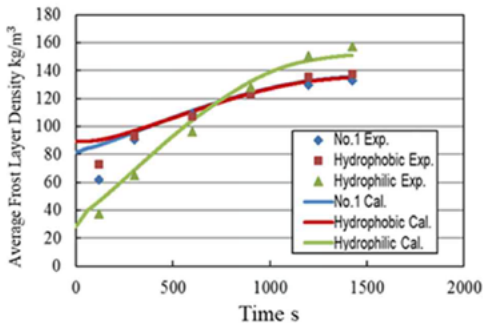

Fig.27. Average Frost Layer Density as Function of Time (2st)

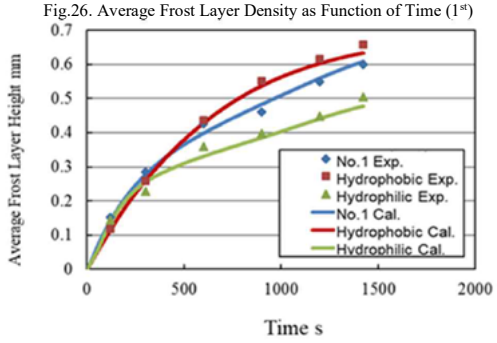

Fig.28. Average Frost Layer Height as Function of Time (1st)

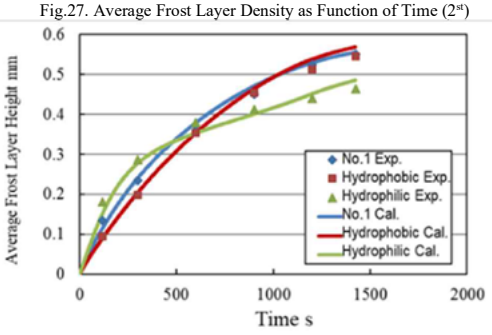

Fig.29. Average Frost Layer Height as Function of Time (2nd)

From Fig. 26. to Fig. 29, it is confirmed the difference between experimental value and calculated value in crystal growth stage are large. Therefore, it is necessary to improve accuracy of the analysis model of this stage.

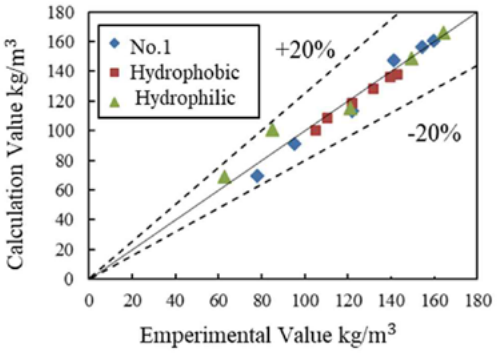

Fig. 30. Error Band of Frost Layer Density (1st)

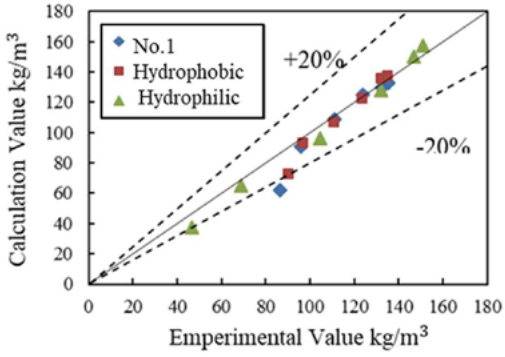

Fig. 31. Error Band of Frost Layer Density (2nd)

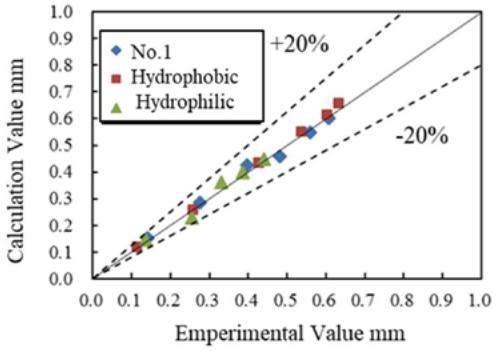

Fig.32. Error Band of Frost Layer Height (1st)

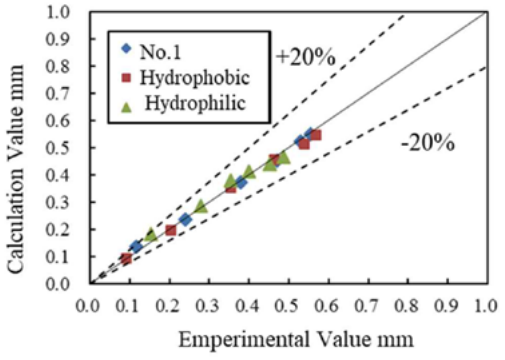

Fig. 33. Error Band of Frost Layer Height (2nd)

From Fig. 30. to Fig.33. show the error band of frost layer density and frost layer height, respectively. Table 6 shows the average error rate.

Table 6 Average Error Band

	No.1		Hydrophobic		Hydrophilic	
	1st	2nd	1st	2nd	1st	2nd
Ave. Frost Density	5.91%	8.79%	3.15%	2.23%	7.48%	5.92%
Ave. Frost Height	4.27%	4.04%	6.09%	3.01%	10.1%	5.95%

From Fig. 30. to Fig. 33., the error band of calculated value is about 10%. Particularly, the average error band is about 2% in No.1.

4. Conclusion

(1) A multi-cycle frost and defrost experiment using a water-cooled jacket is established, and the qualitative frost and defrost characteristics are grasped.
(2) By frost layer growth observation in multi-cycle experiments, the growth of crystal such as initial crystal diameter and spacing is determined, and the effects of convex height and wettability on crystal growth are confirmed.
(3) The calculation results of the analytical model of the frost layer growth on the convex-concave plate are summarized with an error of less than 10% on average, using experimental values as the setting values in the calculation.

(4) Within the scope of this study, the combination of No. 1 plate and the hydrophobic surface treatment had the most frost resistance.

5. Reference

[1] Adachi T, Mizushima J. 1998, The transfer to the stability and the turbulent flow of a flow in rectangular tube. *RIMS Kokyuroku published*. 1051: p. 202-214.

[2] Adachi T, Uehara H. 2000, Pressure Drop and Heat Transfer Characteristics of Flow in Channels with Periodically Grooved Parts, *Transactions of the JSME*. B67(657).

[3] Yang D. 2006, Frost formation on a cold surface under turbulent flow, *International Journal of Refrigeration*. 29(2): p. 164-169.

[4] Yasui K., Katsuta M., Doshida H. and Miyashita R., Study on the Frosting Phenomena between Concavity and Convexity Plate under Forced Convection-Detailed Observation and Analysis of Frost Layer Grouth-,*12th IEA Heat Pump Conference*, Rotterdam Netherland, (2017.5.15).

[5] Tao Y, Besant R, Mao Y. 1993, Characteristics of frost growth on a flat plate during the early growth period. *ASHRAE Transactions*. 99: p. 746-753.

[6] Tao Y, Besant R, Mao Y. 1994, Frost growth characteristics on heat exchanger surface: measurement and simulation. *HTD*, 286: p. 29-38.

[7] Yamashita K. 2009, Frosting phenomenon in low temperature environments. *Doctor's degree of Tamagawa University*.

[8] Fukusako S, Inaba H. 1996, *Heat transfer phenomenon under the cool temperature environment and applicability*. Yokendo, Tokyo, 14 p.

[9] Le Gall, J.M. Grillot and C. Jallut, "Modelling of Frost Growth and Densification", I*nt. J. of Heat Mass Transfer.* 28, (7) (1997),3177-3187.